Journal of Solid State Chemistry **164,** 60–70 (2002)
doi:10.1006/jssc.2001.9448, available online at http://www.idealibrary.com on IDEAL®

Substitutional Effects of 3*d* Transition Metals on the Magnetic and Structural Properties of Quasi-Two-Dimensional $La_5Mo_4O_{16}$

K. V. Ramanujachary,* S. E. Lofland,* W. H. McCarroll,† T. J. Emge,‡ M. Greenblatt,‡ and M. Croft§

*Department of Chemistry and Physics, Rowan University 201 Mullica Hill Road, Glassboro, New Jersey 08028; †Department of Chemistry, Rider University, 2083 Lawrenceville Road, Lawrenceville, New Jersey 08648; ‡Department of Chemistry and Chemical Biology, Rutgers, The State University of New Jersey, 610 Taylor Road, Piscataway, New Jersey 08854; and §Department of Physics, Rutgers, The State University of New Jersey, Piscataway, New Jersey 08855

Received July 10, 2001; in revised form October 25, 2001; accepted November 9, 2001

Substituted phases with the composition $La_5Mo_{4-x}T_xO_{16-\delta}$ (T = Co, Fe, Mn, and Mg and $x \sim 0.7$) were prepared by fused-salt electrolysis and/or conventional solid-state methods. The crystal structure of the parent compound, $La_5Mo_4O_{16}$, contains perovskite-like corner-sharing MoO_6 octahedral units in the *ab* plane separated by Mo_2O_{10} bioctahedral units along the *c* direction. Detailed single-crystal X-ray diffraction studies on the Co-substituted phase, $La_5Mo_{3.31}Co_{0.69}O_{16-\delta}$, indicated that the unit cell is triclinic (space group *C*-1) with Co exclusively replacing Mo atoms in the perovskite layers. X-ray absorption measurements revealed that the transition metal ions are divalent, consistent with the crystal structure analysis. The anomalous magnetic transition observed at 180 K in the parent compound shifts to lower temperatures upon substitution with transition metal ions. No long-range magnetic order was evident in the Mg^{2+}-substituted compositions. The electrical resistivity of all the substituted phases was at least 3 orders of magnitude higher than that of the parent compound. Variations in the magnetic and electrical properties have been ascribed to the disruption of exchange correlations caused by substitutional disorder at the Mo sites.

INTRODUCTION

$La_5Mo_4O_{16}$ is a quasi-two-dimensional (2D) compound containing perovskite-like MoO_3 layers sandwiched between insulating Mo_2O_{10} clusters (1). The perovskite layers and their linking by the edge-sharing bioctahedral clusters are shown in Figs. 1 and 2. Bond valence sums show that Mo(2) and Mo(3) in the perovskite layers have oxidation states of approximately 5+ and 4+, respectively.[1] The Mo_2O_{10} cluster, shown in Fig. 3, contains an unusually short Mo(1)–Mo(1) bond of 2.406 Å where the average Mo oxidation state is 4+. At 180 K the compound undergoes a sharp increase in resistivity accompanied by an unusual anomaly in the magnetic susceptibility, which is not fully understood. The effect is highly anisotropic (Fig. 4) and can be interpreted in terms of magnetic ordering of Mo spins in the perovskite layers (2, 3). Recently Wiebe *et al.* (4) reported on the synthesis and structure of the compound $La_5Re_3MnO_{16}$ which is essentially isomorphous with the title compound where the Mo(3) positions are now occupied by Mn^{2+}. The magnetic susceptibility of this compound, as measured on a polycrystalline sample, displays a behavior similar to that shown in Fig. 4a for polycrystalline $La_5Mo_4O_{16}$.

Several years ago, during attempts to prepare $LaCoO_3$ by fused-salt electrolysis (FSE) in alkali molybdate solvents, we noted the formation of $La_5Mo_4O_{16}$-like crystals at the cathode. Since we were interested in potentially colossal magnetoresistive materials that might be produced at the anode and because $La_5Mo_4O_{16}$ would not be an unexpected reduction product, the observation was not pursued further until Wiebe *et al.*'s report (4). A careful analysis of the powder X-ray diffraction pattern (XRD) of this cathode product revealed an apparent modification of the parent compound, indicating that some Co substitution had probably taken place. A chemical analysis of the crystals indicated a chemical formula close to $La_5Mo_{3.25}Co_{0.75}O_{16}$. However, the analysis was complicated by the fact that Co metal inclusions were present in most of the crystals, indicating that the actual amount of Co substitution into the crystals would be somewhat lower. This was confirmed by the results of a single-crystal structural analysis presented below. We have also examined the possibility that Co^{2+} may be replaced by other divalent metals with solid-state reactions and found that this was also possible for Mg, Fe, Mn, and Ni. Data regarding the magnetic properties of

[1]The numbering of the atoms in Figs. 1–3 differs from that used in Ref. (1).

0022-4596/02 $35.00

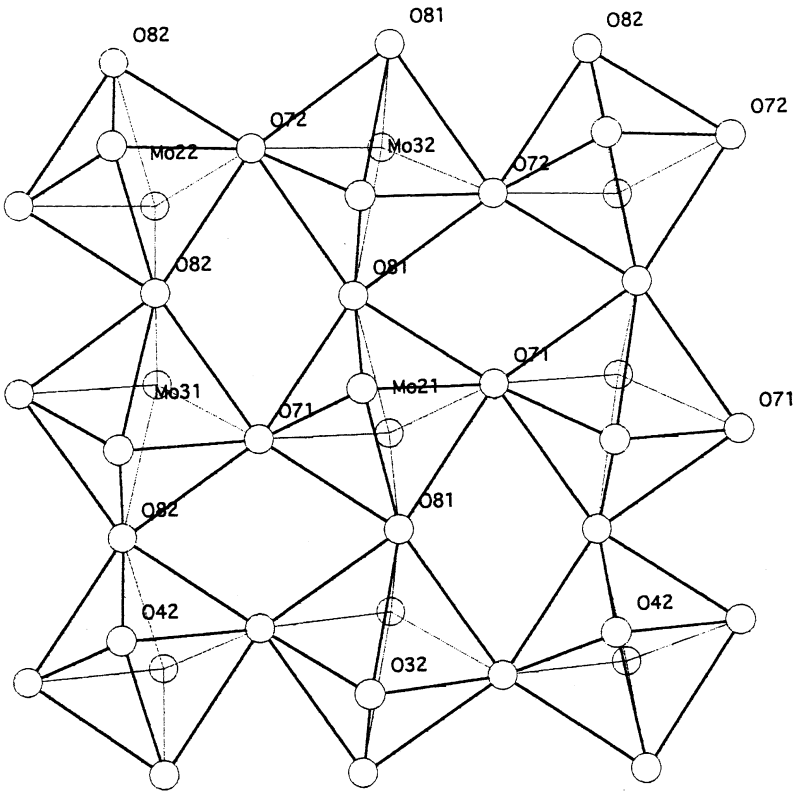

FIG. 1. Perovskite-like layers in the *ab* plane of $La_{5.00}Mo_{3.31}Co_{0.69}O_{15.8}$ ([110] projection).

these phases along with supporting X-ray absorption spectra (XAS) for transition metal valence assignments are also presented.

EXPERIMENTAL

Synthesis and Chemical Analysis

All reagents used in these experiments were of reagent grade or 99.99% purity except the MoO_2 which had been obtained from RIC-ROC and was about 15 years old. This once pure material had undergone slight oxidation in the intervening years and its recent XRD pattern showed several lines corresponding to Mo_4O_{11}, in addition to several very weak unidentified lines. It could be rendered pure to X rays by treatment in hot, 1 F NaOH for several hours, washing by decantation, and being allowed to stand at room temperature in 0.5 F HCl overnight before filtering and washing with water, dilute NH_4OH, water, and acetone. $MnCO_3$ was prepared using standard methods by precipitation from solutions of manganese(II) nitrate and ammonium carbonate. Co_3O_4 was prepared by FSE in this laboratory, Mn_3O_4 was prepared by heating reagent grade MnO_2 overnight in air at 970°C, and Mn_2O_3 was prepared by treating Mn_3O_4 in oxygen at 725°C for 36 hours. The weight change corresponded to 99.95% conversion. MgO was prepared from $MgCO_3$ by ignition in air at 800°C for several hours.

The general details of the fused-salt electrolysis (FSE) method used here have been described previously (5, 6). The successful synthesis of crystals of a cobalt-substituted phase was accomplished using a melt prepared from a 35-g mixture with the initial molar composition Na_2MoO_4:MoO_3:La_2O_3:$CoCO_3$ = 2.60:1.00:0.350:0.015–0.025. The mix was contained in a 25-ml Vesuvius yttria-stabilized zirconia crucible. The electrolyses were carried out at 980–1000°C with Pt electrodes for periods of 2–24 hours employing currents of 20–35 mA. The initial runs produced small quantities (several milligrams) of an unidentified needle-like, cobalt-containing product but eventually, the desired plate-like crystals grew at the cathode in yields of approximately 0.1–0.2 g per overnight run. These were freed from the matrix by washing with a warm solution containing 5% and 2% by weight of potassium carbonate and ethylenediaminetetraaceticacid, respectively. The crystals ranged in size from 0.1 to 2.0 mm on edge and most contained either a sparse, thin, granular coating of Co or occasional inclusions of Co fibers. When approximately half of the initial Co had been removed from the melt (as judged by subsequent chemical analysis), the production of crystals on the cathode

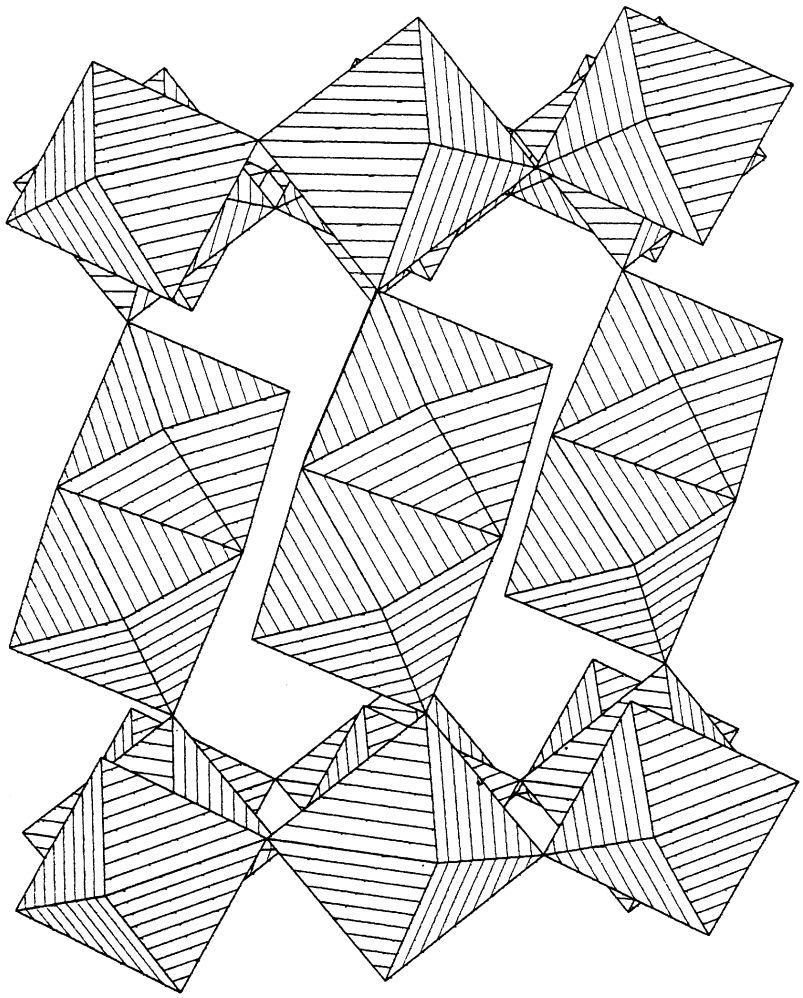

FIG. 2. Mo–O and Co–O network in $La_{5.00}Mo_{3.31}Co_{0.69}O_{15.8}$ showing the linkage of perovskite layers by Mo_2O_{10} clusters.

ceased. Crystal growth could be restarted by adding several milligrams of Co_3O_4 to the melt.

Attempts to grow crystals containing Fe, Mn, and Ni by replacing the $CoCO_3$ by Fe_2O_3, Mn_2O_3, or NiO and by otherwise retaining the same approximate melt conditions were not successful. Variations in the La_2O_3 to 3*d* transition metal oxide ratio had no beneficial effects.

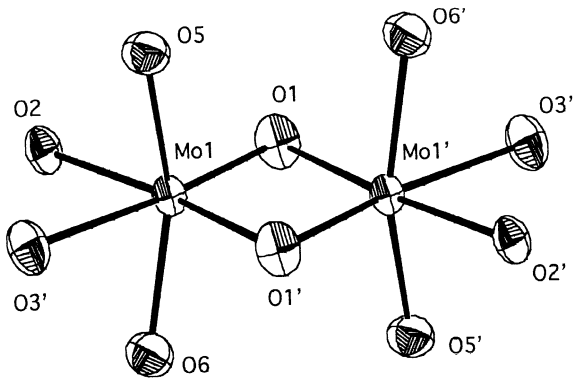

FIG. 3. ORTEP diagram of the Mo_2O_{10} cluster in $La_{5.00}Mo_{3.31}Co_{0.69}O_{15.8}$ (70% probability level).

Polycrystalline samples with the compositions $La_5Mo_{4-x}T_xO_{15-y}$ ($x = 0.0$–0.75, $y = 0.0$–0.75, $T^{2+} =$ Mg, Mo, Fe, Co, Ni) were prepared by heating the intimately mixed, pelleted, constituent oxides of the desired end product stoichiometry in evacuated sealed silica capsules for 3 days at 1000°C or 1100°C followed by regrinding, repelleting, and further heat treatment *in vacuo* at 1200°C for 3 days. The nominal oxygen content was fixed by the ratio of MoO_3:MoO_2 employed in the starting mixtures.

Chemical analysis to establish the composition of the cobalt-containing crystals and the Co content of the partially depleted melt were carried out with a Baird atomic inductively coupled plasma emission spectrometer using matrix-matched standards. The results are considered accurate to approximately $\pm 1\%$ by weight. Results of chemical analysis of the crystals were as follows: La, 53.1%; Mo,

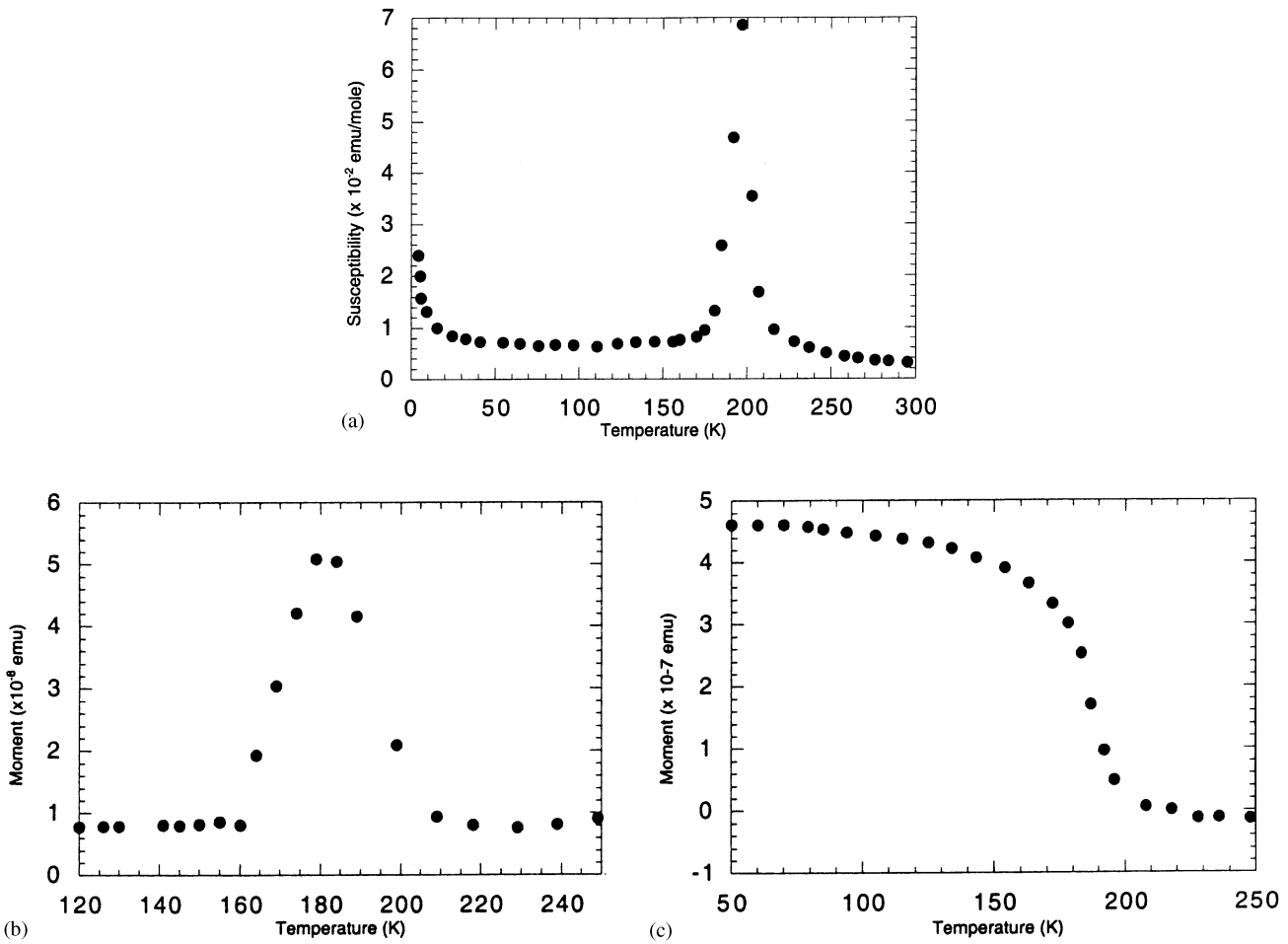

FIG. 4. Magnetic susceptibility vs temperature for $La_5Mo_4O_{16}$: (a) randomly oriented crystals, (b) field perpendicular, and (c) parallel to the perovskite-like layers.

23.9%; Co, 3.32% by weight. Calculated for $La_5Mo_{3.31}Co_{0.69}O_{15.8}$: La, 53.2%; Mo, 24.3%; Co, 3.11%.

Physical Measurements

X-ray diffraction. Powder X-ray diffraction studies were carried out with a Rigaku D-Max2 system on a horizontal goniometer that employed graphite-monochromatized Cu$K\alpha$ radiation. Mo was used as an internal standard for data used for measurements of lattice parameters which were refined by a least-squares method (7).

Single-crystal X-ray diffraction data for a cobalt-substituted crystal of $La_5Mo_4O_{16}$ were collected on a Nonius CAD4 diffractometer with graphite-monochromatized Mo$K\alpha$ ($\lambda = 0.7107$ Å) radiation. The three check reflections measured every hour showed less than 1% intensity variation. The data were corrected for Lorenz effects and polarization as well as absorption, the latter by a numerical method (8). The unit cell parameters were determined from 25 centered reflections in the range $11.4^\circ < 2\theta < 14.6^\circ$ (7) and are given in Table 1.

At first, α and γ were observed to be $\sim 90.00^\circ$, and the crystal symmetry appeared to be monoclinic as reported for $La_5Mo_4O_{16}$. However, averaging of reflection data collected in the complete sphere to the limit $\theta = 30^\circ$in the $2/m$ Laue symmetry did not yield an acceptable R_{sym}. Subsequent refinement of the triclinic model initially based upon the reported atomic coordinates of $La_5Re_3MnO_{16}$, with a twinning mirror perpendicular to the crystallographic b axis and a 0.528:0.472(2) ratio of twin components, gave suitable results (see Table 1). All atom coordinates, anisotropic displacement parameters, as well as the twin, overall scale and equivalent isotropic extinction factors were refined with full-matrix least-squares methods (9). The third Mo atom site (Mo(3) in Table 2) was best modeled with a 0.687:0.313(9) mixture of Co and Mo, respectively. The other two Mo sites were completely occupied with Mo atoms. All La sites were found to be fully

TABLE 1
Crystal Data and Structure Refinement for $La_5Mo_{3.31}Co_{0.69}O_{15.8}$

Empirical formula	$La_{5.0}Mo_{3.31}Co_{0.69}O_{15.8}$
Formula weight	1305.04
Temperature	293(2) K
Wavelength	0.7107 Å
Crystal system, space group	Triclinic, *C*-1
Unit cell dimensions	$a = 7.9689(3)$ Å, $b = 7.9398(5)$ Å, $c = 10.3554(9)$ Å $\alpha = 90.000(6)^\circ$, $\beta = 95.119(5)^\circ$, $\gamma = 89.984(4)^\circ$
Twinning matrix	$\{1\,0\,0;\ 0\,\bar{1}\,0;\ 0\,0\,1\}$
Volume	652.59(7) Å^3
Z, calculated density	2, 6.645 Mg/m^3
Absorption coefficient	19.984 mm^{-1}
F(000)	1138
Crystal size	0.110 × 0.080 × 0.066 mm
Theta range for data collection	3.63 to 44.91°
Limiting indices	$-11 \le h \le 15,\ -15 \le k \le 15,\ -20 \le l \le 20$
Reflections collected/unique	7344/5328 [R(int) = 0.0116]
Completeness to $\theta = 44.91$	99.9%
Absorption correction	Numerical
Max. and min. transmission	0.3177 and 0.2201
Refinement method	Full-matrix least-squares on F^2
Data/restraints/parameters	5328/174/122
Goodness-of-fit on F^2	1.009
Final R indices [$I > 2\sigma(I)$]	$R1 = 0.0316$, w$R2 = 0.0825$
R indices (all data)	$R1 = 0.0338$, w$R2 = 0.0838$
Extinction coefficient	0.00423(14)
Largest diff. peak and hole	4.5 and −4.3 e.Å^{-3}

occupied. The occupancies of the O atoms were refined, and only atom O(7) was found to significantly differ (e.g., above the 3σ level) from unity, at 0.92(2). Crystallographic data and final R indices for $La_5Mo_{3.31}Co_{0.69}O_{15.8}$ are given in Table 1. Atomic coordinates, equivalent isotropic displacement parameters, and site occupancies are given in Table 2. Selected bond distances and angles are given in Table 3.

TABLE 2
Atomic Coordinates (×10^4) and equivalent Isotropic Displacement Parameters (Å×10^3) for $La_5Mo_{3.31}Co_{0.69}O_{15.8}$

Atom	*x*	*y*	*z*	*U*(eq)[a] Site	Occup.
La(1)	2260(1)	7490(1)	8018(1)	9(1)	1.0
La(2)	2249(1)	2610(1)	7947(1)	8(1)	1.0
La(3)	5000	5000	5000	8(1)	1.0
Mo(1)	603(1)	4991(1)	3931(1)	4(1)	1.0
Mo(2)	0	0	0	5(1)	1.0
Co(3)	0	5000	0	5(1)	0.687(9)
Mo(3)	0	5000	0	5(1)	0.313(9)
O(1)	1870(3)	5001(6)	5656(2)	7(1)	1.0
O(2)	2850(3)	5010(6)	3248(2)	6(1)	1.0
O(3)	−403(3)	4981(6)	1919(2)	8(1)	1.0
O(4)	718(4)	37(7)	1768(3)	11(1)	1.0
O(5)	399(5)	7352(5)	3605(3)	7(1)	0.959(19)
O(6)	428(5)	2640(5)	3613(3)	8(1)	1.0
O(7)	−528(5)	2473(4)	−8(3)	9(1)	0.918(18)
O(8)	2392(4)	480(5)	−384(3)	10(1)	1.0

[a] U(eq) is defined as one-third of the trace of the orthogonalized U_{ij} tensor.

TABLE 3
Bond Lengths (Å) and Angles (°) for $La_5Mo_{3.31}Co_{0.69}O_{15.8}$

La(1)–O(2)#1	2.375(4)	La(1)–O(3)#2	2.463(4)
La(1)–O(4)#3	2.570(5)	La(1)–O(7)#4	2.578(4)
La(1)–O(7)#2	2.581(4)	La(1)–O(6)#2	2.609(4)
La(1)–O(5)#1	2.623(4)	La(1)–O(8)#5	2.890(4)
La(1)–O(4)#2	3.103(4)	La(1)–O(1)	3.138(4)
La(1)–O(3)#1	3.206(4)	La(1)–O(8)#3	3.395(3)
La(2)–O(8)#6	2.413(3)	La(2)–O(2)#3	2.418(4)
La(2)–O(3)#2	2.424(4)	La(2)–O(4)#3	2.474(5)
La(2)–O(5)#2	2.535(4)	La(2)–O(6)#3	2.570(4)
La(2)–O(8)#3	2.937(4)	La(2)–O(1)	3.032(3)
La(2)–O(4)#7	3.197(4)	La(2)–O(7)#6	3.199(4)
La(2)–O(7)#3	3.224(4)	La(2)–O(3)#3	3.241(4)
La(3)–O(2)	2.382(2)	La(3)–O(2)#8	2.382(2)
La(3)–O(6)#9	2.581(4)	La(3)–O(6)#3	2.581(4)
La(3)–O(5)#1	2.586(4)	La(3)–O(5)#10	2.586(4)
La(3)–O(1)	2.643(2)	La(3)–O(1)#8	2.643(2)
La(3)–O(4)#9	3.445(3)	La(3)–O(4)#3	3.445(3)
Mo(1)–O(6)	1.898(4)	Mo(1)–O(5)	1.910(4)
Mo(1)–O(1)	1.972(3)	Mo(1)–O(2)	1.983(2)
Mo(1)–O(1)#2	2.054(2)	Mo(1)–O(3)	2.164(3)
Mo(1)–Mo(1)#2	2.4920(5)		
Mo(2)–O(4)	1.869(3)	Mo(2)–O(4)#11	1.869(3)
Mo(2)–O(7)#11	2.008(3)	Mo(2)–O(7)	2.008(3)
Mo(2)–O(8)#11	2.018(3)	Mo(2)–O(8)	2.018(3)
Co(3)–O(3)	2.041(3)	Co(3)–O(3)#12	2.041(3)
Co(3)–O(7)	2.050(3)	Co(3)–O(7)#12	2.050(3)
Co(3)–O(8)#13	2.116(3)	Co(3)–O(8)#14	2.116(3)
O(6)–Mo(1)–O(5)	158.61(11)		
O(6)–Mo(1)–O(1)	100.66(17)	O(5)–Mo(1)–O(1)	100.63(17)
O(6)–Mo(1)–O(2)	90.05(17)	O(5)–Mo(1)–O(2)	89.70(17)
O(1)–Mo(1)–O(2)	85.28(10)	O(6)–Mo(1)–O(1)#2	88.96(18)
O(5)–Mo(1)–O(1)#2	88.02(18)	O(1)–Mo(1)–O(1)#2	103.55(9)
O(2)–Mo(1)–O(1)#2	171.15(10)	O(6)–Mo(1)–O(3)	79.32(16)
O(5)–Mo(1)–O(3)	79.34(16)	O(1)–Mo(1)–O(3)	171.01(10)
O(2)–Mo(1)–O(3)	85.74(10)	O(1)#2–Mo(1)–O(3)	85.44(10)
O(6)–Mo(1)–Mo(1)#2	97.56(11)	O(5)–Mo(1)–Mo(1)#2	96.76(11)
O(1)–Mo(1)–Mo(1)#2	53.25(7)	O(2)–Mo(1)–Mo(1)#2	138.52(7)
O(1)#2–Mo(1)–Mo(1)#2	50.30(7)	O(3)–Mo(1)–Mo(1)#2	135.74(7)

Symmetry transformations used to generate equivalent atoms: #1, $-x+\frac{1}{2}, -y+\frac{3}{2}, -z+1$; #2, $-x, -y+1, -z+1$; #3, $-x+\frac{1}{2}, -y+\frac{1}{2}, -z+1$; #4, $x+\frac{1}{2}, y+\frac{1}{2}, z+1$; #5, $x, y+1, z+1$; #6, $x, y, z+1$; #7, $-x, -y, -z+1$; #8, $-x+1, -y+1, -z+1$; #9, $x+\frac{1}{2}, y+\frac{1}{2}, z$; #10, $x+\frac{1}{2}, y-\frac{1}{2}, z$; #11, $-x, -y, -z$; #12, $-x, -y+1, -z$; #13, $x-\frac{1}{2}, y+\frac{1}{2}, z$; #14, $-x+\frac{1}{2}, -y+\frac{1}{2}, -z$; #15, $x-\frac{1}{2}, y-\frac{1}{2}, z$; #16, $x-\frac{1}{2}, y-\frac{1}{2}, z-1$; #17, $x, y, z-1$; #18, $x, y-1, z-1$.

Magnetic properties. DC magnetization measurements of randomly oriented single crystals were carried out with a Squid magnetometer (Quantum Design, MPMS). AC/DC magnetization and their field dependence of the polycrystalline samples were recorded with a Quantum Design physical property measurement system (PPMS). For AC measurements a frequency of 1000 Hz and an amplitude of ~10 G were applied. Data were recorded at various temperatures in the interval 1.5–400 K at applied magnetic

fields in the range 0.1–9 Tesla. Corrections due to the core diamagnetism of the constituent ions were not applied in view of their negligible contribution relative to the total moment.

Electrical properties. Electrical resistivity of $La_5Mo_{3.31}Co_{0.69}O_{15.8}$ single crystals was measured in a four-probe configuration with the current parallel to the *ab* plane. Ohmic contacts were made by attaching fine copper leads to the crystal with silver paint.

X-ray absorption spectroscopy (XAS). The Mo $L_{2,3}$-edge and Co *K*-edge X-ray absorption spectroscopy (XAS) measurements were performed on beam line X-19A at the Brookhaven National Synchrotron Light Source with a double-crystal [Si(111)] monochromator. The XAS measurements were made in the electron yield and fluorescence modes for Mo and in the transmission and fluorescence modes for the Co. For the Co XAS measurements a standard was run simultaneously for a precise energy calibration of the Co spectra to a relative accuracy of about 0.03 eV. Standard samples were run frequently in the Mo measurements for calibration with a lower accuracy of about 0.1 eV. The spectral data were treated by subtracting the linear energy-dependent background before the edge, yielding a constant average absorption coefficient step 100 eV above the edge. As is conventional, this absorption coefficient step was normalized to unity.

RESULTS AND DISCUSSION

Structural Properties

Figure 1 is a projection of the crystal structure of $La_5Mo_{3.31}Co_{0.69}O_{15.8}$ along the [001] direction that clearly shows the nature of the perovskite-like layer. The Mo(3) site is now occupied by Co as well as Mo in a ratio of 0.69/0.31. Figure 2 shows how the perovskite layers are separated by the Mo_2O_{10} clusters, thus giving rise to the quasi-low-dimensional character of this phase.

The results of the chemical analysis of the cobalt-containing crystals showed the metals to be in the molar ratios La:Mo:Co = 5.00:3.26:0.74. However, since the crystals were contaminated with a small amount of Co metal, the true Mo:Co ratio in the compound must be somewhat higher. In addition, there is some evidence that Co may replace Mo over a range of compositions. This appears to be born out by the results of the occupancy refinements in the single-crystal X-ray diffraction study, which yielded a probable chemical formula of $La_5Mo_{3.31}Co_{0.69}O_{15.8}$, and we therefore chose this as the best representation of the composition of the crystal used here.

Although the oxygen nonstoichiometry in the cobalt compound is small and, from a diffraction point of view, barely significant, it would seem from a valence point of view to be essential. In $La_5Mo_4O_{16}$ a bond valence analysis showed that Mo(2) and Mo(3), which are found in the perovskite-like layers, are predominantly penta- and tetravalent, respectively, while the Mo(1) atoms, which are strongly bonded to each other in the insulating Mo_2O_{10} clusters, are tetravalent. Given the low-valent nature of the Mo ensemble, it would be expected that the Co, which substitutes solely in the Mo(3) sites, would not have a valence higher than two. If there were no other valence changes, then an oxygen deficiency of 0.7 per formula unit would be required for a Co content of 0.69. That this is not seen is the result of a compensating increase in the average oxidation state of the Mo(1) cluster atoms to approximately 4.5 + . Indeed, aside from the oxygen nonstoichiometry, the principal difference between $La_5Mo_4O_{16}$ and $La_5Mo_{3.31}Co_{0.69}O_{15.8}$ is that the Mo(1)–Mo(1) bond distance in the latter has increased dramatically to 2.496 Å as compared to 2.406 Å in the former.

While the increase in this bond distance itself can be interpreted as evidence for an increase in average Mo oxidation state, a better indication of its magnitude is given by a bond valence analysis of the metal oxygen bonds as suggested by Brown and Wu (10). The results of such an analysis show that the average oxidation state for Mo(1) is 4.47+. That for Mo(2) is found to be 4.76+, reasonably close to the expected value of 5+. The Mo(3) site, which is predominately occupied by Co, has an average oxidation state of 2.55+, 1.53+ coming from Co and 1.02+ coming from Mo. The oxidation states for La(1), La(2), and La(3) are calculated to be 2.97+, 3.12+, and 2.91+, respectively, provided all the La–O bonds listed in Table 3 that are less than 3.25 Å are used in the calculations. If distances greater than 3.11 Å are ignored for La(2), the value would drop to 2.81+. Thus, by assigning oxidation states of 3.0+ to all La, 4.5+ to the cluster Mo(1), pentavalence to Mo(2), tetravalence to Mo(3), and divalence to the Co, we arrive at the chemical formula $La_{5.00}Mo_{3.31}Co_{0.69}O_{15.81}$, whose oxygen content is in remarkable agreement with the X-ray result.

XAS

Further evidence for the assignment of divalence to the Co comes from XAS measurements. Measurements of the Co-*K*-edge for $La_5Mo_{3.31}Co_{0.69}O_{15.8}$ along with elemental Co and Co^{2+}, Co^{3+}, and "4+" standard compounds are shown in Fig. 5. Note the coincidence between the Co^{2+} standard and the Mo compound spectra at the edge-onset energy (see box 1 in the figure) and the steeply rising portion of the edge energy (box 2). This coincidence clearly supports a Co^{2+} state in the Mo compound.

The top portion of Fig. 6 shows the Mo L_3-edges for a series of elemental Mo and Mo^{4+}, Mo^{5+}, and Mo^{6+} standards. The Mo L_3 transitions involve empty Mo *d* final states and therefore provide a probe of the empty *d*

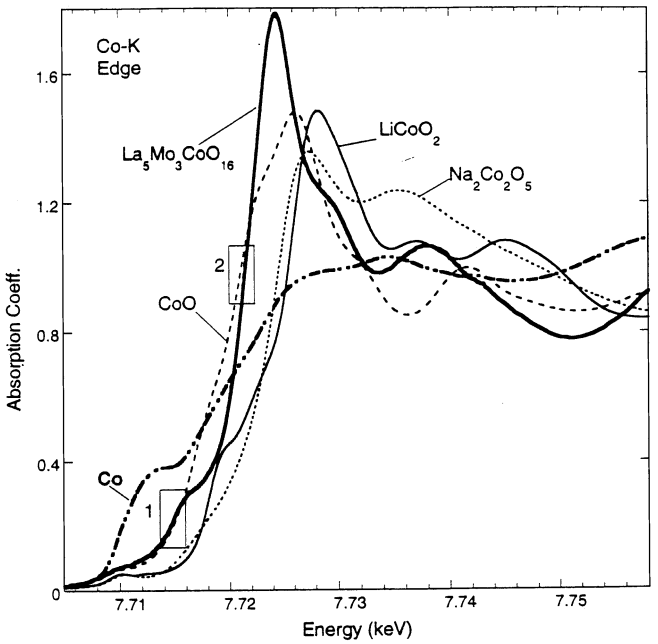

FIG. 5. Co *K*-edge XAS for $La_{5.00}Mo_{3.31}Co_{0.69}O_{15.8}$ along with a series of Co standard compounds.

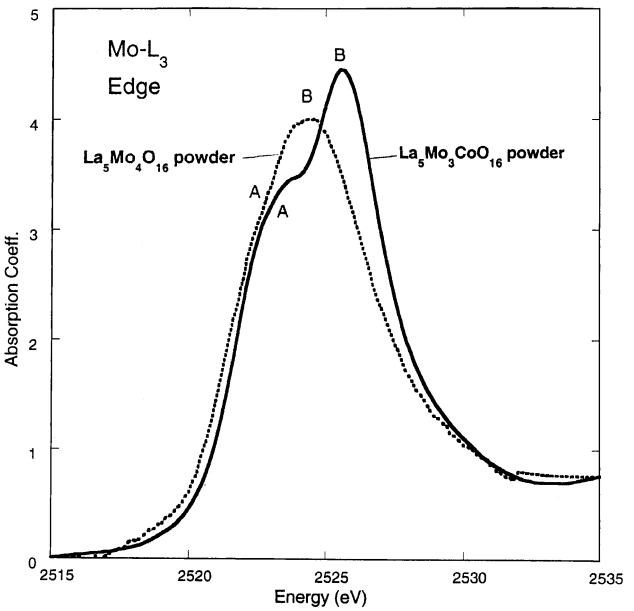

FIG. 7. Comparison of the Mo L_3-edges for $La_5Mo_4O_{16}$ and $La_{5.00}Mo_{3.31}Co_{0.69}O_{15.8}$ powders.

density-of states (modified by matrix element and atomic multiplet effects). The *A* and *B* features on MoO_3, for example, are respectively associated with t_{2g} and e_g Mo *d* final states. The intensity of the *A* feature (see Fig. 6) increases systematically with increasing *d*-hole count (valence). Also note that the centrum of the *A*–*B* feature group typically exhibits a chemical shift to higher energy with increasing valence. The Mo L_3-edges for $La_5Mo_4O_{16}$ samples in powder form and for a collage of crystal platelets oriented so that the photon polarization vector is aligned in the platelet plane are shown in the bottom portion of Fig. 6. The crystal spectrum is sensitive to d-orbital hole states oriented in this plane. The overall Mo spectrum supports a Mo oxidation state (averaged over all sites) well above 4+ but less than 5+.

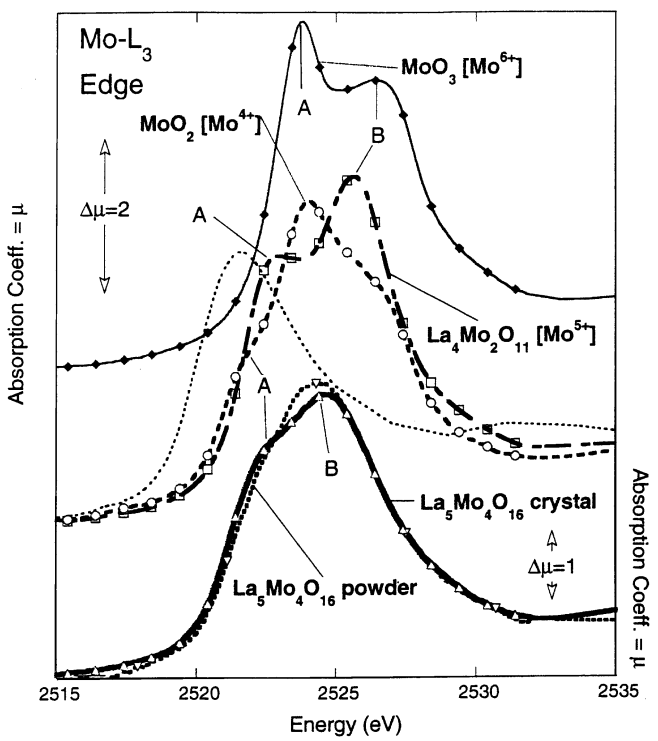

FIG. 6. Mo L_3 XAS for standards (top) and for $La_5Mo_4O_{16}$ in powder form and as a partially oriented collage (bottom).

Figure 7 shows a comparison of the Mo L_3-edges for powdered samples of $La_5Mo_4O_{16}$ and $La_5Mo_{3.31}Co_{0.69}O_{15.8}$. The Co-substituted compound manifests a dramatically sharper, more intense *A* feature and an overall shift to higher energy. This strongly supports a dramatic Mo valence increase accompanying Co substitution. Figure 8 is a comparison of the Mo L_3-edges for crystal platelet collages of $La_5Mo_4O_{16}$ and $La_5Mo_{3.31}Co_{0.69}O_{15.8}$ oriented with the beam polarization vector in the *ab* crystal plane. The Co-induced changes in the in-plane Mo *d* density-of-states are spectacular. Specifically, the Co-substitution-induced Mo *d* holes have a strong in-*ab*-plane character.

Since our attempts to prepare other 3*d*-substituted transition metal phases by FSE were unsuccessful, we thought it would be worthwhile to see if other substitutions could be effected using solid-state reactions. This was done while the crystal structure determination on the Co compound was in progress and, because we were not aware of

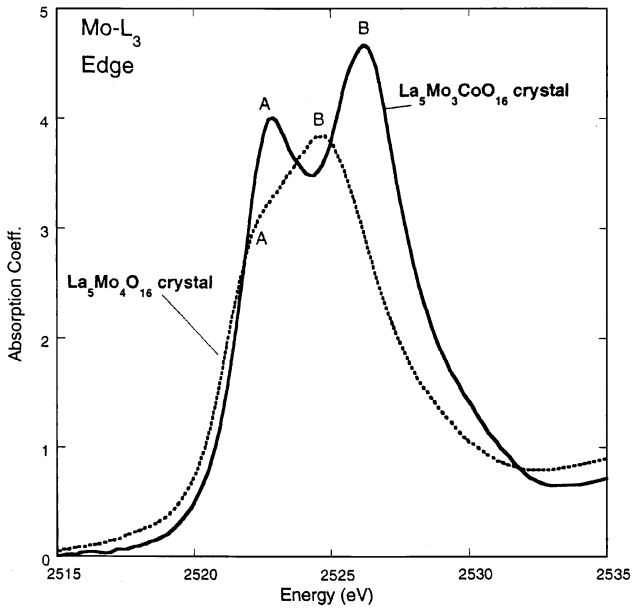

FIG. 8. Comparison of the Mo L_3-edges for $La_5Mo_4O_{16}$ and $La_{5.00}Mo_{3.31}Co_{0.69}O_{15.8}$ single-crystal platelet samples with *c*-axial preferred orientation (i.e., beam polarization in the *ab* plane).

the dramatic change in the average oxidation state of Mo(1) which occurs when Co is substituted, we assumed that the use of this divalent ion would probably be accompanied by a significant decrease in the oxygen content. We therefore initially investigated the compositions $La_{5.00}Mo_{3.25}T_{0.75}O_{15.25}$ and $La_{5.00}Mo_{3.25}T_{0.75}O_{15.375}$ (T = Mg, Mn, Fe, Ni, and Co) by this method. Summaries of these results are given in Table 4. We found that for Mn, Fe, and Co the major phase seen in the XRD for the compositions $La_{5.00}Mo_{3.25}T_{0.75}O_{15.25}$ was the modified $La_5Mo_4O_{16}$ type although a few weak lines of both $La_5Mo_3O_{16}$ and $La_{16}Mo_{21}O_{56}$ were noted. For these ions when the composition was $La_{5.00}Mo_{3.25}T_{0.75}O_{15.375}$, the impurity lines were weaker and in the case of the Co compound, it appeared to be "X-ray pure". However, this latter phase was ferromagnetic and contained Co metal as did all Co phases, which we attempted to prepare in this fashion. When Mg was used as the substituent, significant amounts of $La_5Mo_3O_{16}$ were seen in the XRD for both compositions. In the case of the Ni-containing phases, $La_5Mo_3O_{16}$ appeared to be the major constituent and the presence of Ni metal was clearly evidenced, both visually and by its strong ferromagnetism.

TABLE 4
Unit Cell Constants and Other Data for $La_5Mo_{4-x}T_xO_{15-y}$ Phases

Formula	a (Å)	b (Å)	c (Å)	β (°)	V(Å^3)	Prep. conditions	Purity
$La_5Mo_{3.25}Mg_{0.75}O_{15.25}$	7.967(2)	7.961(2)	10.348(3)	95.12(2)	653.7(2)	3da-1000 + 3da-1200°C	Impure
$La_5Mo_{3.25}Mn_{0.75}O_{15.25}$	7.999(2)	7.965(2)	10.391(2)	95.18(2)	659.4(2)	3da-1000 + 3da-1200°C	Impure
$La_5Mo_{3.25}Fe_{0.75}O_{15.25}$	7.961(1)	7.952(2)	10.311(1)	95.02(1)	650.2(1)	3da-1000 + 3da-1200°C	Several weak imp. lines
$La_5Mo_{3.25}Co_{0.75}O_{15.25}$	7.977(2)	7.961(2)	10.335(1)	95.07(1)	653.7(1)	3da-1000 + 3da-1200°C	X-ray pure, but magnetic
$La_5Mo_{3.25}Ni_{0.75}O_{15.25}$	7.967(2)	7.973(3)	10.335(3)	94.99(1)	654.1(3)	3da-1000 + 3da-1200°C	Very impure (5316) and highly magnetic
$La_5Mo_{3.25}Mn_{0.75}O_{15.375}$	8.000(1)	7.965(1)	10.382(1)	95.01(1)	659.0(1)	3da-1000 + 3da-1200°C	4 very weak impurity lines in XRD
$La_5Mo_{3.25}Fe_{0.75}O_{15.375}$	7.963(2)	7.962(2)	10.312(2)	95.06(1)	651.3(2)	3da-1000 + 3da-1200°C	One 162156 line in XRD
$La_5Mo_{3.25}Co_{0.75}O_{15.375}$	7.979(1)	7.959(11)	10.345(1)	95.11(1)	654.3(1)	3da-1000 + 3da-1200°C	1 vvw line 211 + sl. magnetic
$La_5Mo_{3.25}Ni_{0.75}O_{15.375}$	7.968(6)	7.973(8)	10.334(7)	94.99(2)	654.1(5)	3da-1000 + 3da-1200°C	Very impure (5316) and highly magnetic
$La_5Mo_{3.30}Mg_{0.70}O_{15.8}$	7.964(1)	7.950(1)	10.356(2)	95.09(1)	653.1(1)	3da-1000 + 3da-1200°C	1 vv (5316) + 1 weak line
$La_5Mo_{3.30}Mn_{0.70}O_{15.8}$	7.995(1)	7.968(1)	10.380(1)	95.21(1)	658.5(1)	3da-1000 + 3da-1200°C	X-ray pure
$La_5Mo_{3.30}Fe_{0.70}O_{15.8}$	7.9631(1)	7.975(1)	10.305(1)	95.00(1)	651.9(1)	3da-1000 + 3da-1200°C	X-ray pure
$La_5Mo_{3.30}Co_{0.70}O_{15.8}$	7.980(1)	7.947(1)	10.355(2)	95.13(1)	654.0(1)	3da-1100 + 3da-1200°C	X-ray pure, but very weakly magnetic
$La_5Mo_{3.3}Ni_{0.7}O_{15.8}$	7.966(2)	7.990(2)	10.327(2)	95.02(2)	654.8(2)	3da-1000 + 3da-1200°C	Very impure (5316) highly magnetic
$La_5Mo_{3.30}Co_{0.70}O_{15.8}$	7.9689(3)	7.9398(5)	10.3554(9)	95.119(5)	652.59(1)	FSE	(single crystal data)
$La_5Mo_4O_{16}$	7.9638(7)	7.9958(5)	10.3345(7)	95.067(6)	655.5(1)	FSE	(single crystal data from Ref. 1)
$La_5Mo_4O_{16}$	7.797(1)	8.002(1)	10.338(2)	95.01(1)	656.8(1)	FSE	(powder data)
$La_5Mo_{3.30}Fe_{0.70}O_{15.91}$	7.964(3)	7.970(3)	10.318(3)	95.06(2)	652.3(2)	6da-1100°C	X-ray pure
$La_5Mo_{3.40}Co_{0.60}O_{15.8}$	7.980(10)	7.947(1)	10.335(1)	95.13(1)	654.0(1)	3da-1000 + 3da-1200°C	X-ray pure but very weakly magnetic
$La_5Mo_{3.40}Co_{0.60}O_{15.40}$	7.980(10)	7.969(1)	10.334(1)	95.09(1)	654.1(1)	3da-1000 + 3da-1200°C	X-ray pure but magnetic
$La_5Mo_{3.70}Co_{0.30}O_{15.70}$	7.978(1)	7.985(1)	10.325(1)	95.06(1)	655.2(1)	3da-1000 + 3da-1200°C	X-ray pure, slightly magnetic

Note: The terms 4211, 5316 and 162156 refer to the compounds $La_4Mo_2O_{11}$, $La_5Mo_3O_{16}$, and $La_{16}Mo_{21}O_{56}$, respectively.

TABLE 5
Variation of Unit Cell Volumes for $La_5Mo_{3.31}Co_{0.69}O_{15.8}$ Phases with Ionic Radii of *T*

Compound	V_{cell} (Å)	Radius of T (Å)
$La_5Mo_4O_{15}$	656.8(2), 655.5[a]	Mo(IV) 0.79 Mo(V) 0.75
$La_5Mo_{3.30}Mg_{0.70}O_{15.8}$	653.1(1)	0.86
$La_5Mo_{3.30}Mn_{0.70}O_{15.8}$	658.9(1)	0.97
$La_5Mo_{3.30}Fe_{0.70}O_{15.8}$	652.3(2)	0.92
$La_5Mo_{3.30}Co_{0.70}O_{15.8}$	654.0(1), 652.59(7)[a]	0.88.5
$La_5Mo_{3.30}Ni_{0.70}O_{15.8}$	654.6(1)	0.83

[a]Single-crystal results for $La_5Mo_{3.31}Co_{0.69}O_{15.8}$.

Subsequently, based upon the results of the single-crystal analysis of the Co compound, we also used solid-state reactions to investigate compositions at or near $La_{5.00}Mo_{3.30}T_{0.70}O_{15.8}$. In the cases of the Mn, Fe, and Co preparations, the phases were X-ray pure (although the Co compound was magnetic) while the Mg compound showed only one very weak impurity line in its XRD pattern. The preparation with Ni was still highly impure as indicated by both its magnetism and XRD. The variations in unit cell volumes for the various phases of a particular T^{2+} ion would seem to indicate that some range of solid solution exists particularly for the phases containing Co^{2+} and Fe^{2+} (Table 4). It is not clear, however, whether this variation is associated with the variation of the T^{2+} ion content or the oxygen content or both. Clearly, further investigation is warranted.

Table 5 lists unit cell volumes for $La_{5.00}Mo_{3.30}T_{0.70}O_{15.8}$ phases and $La_5Mo_4O_{16}$ along with the corresponding Shannon–Prewitt radii (all high spin) (11). Since the T metal substitution increases the relative amount of Mo(V) present in supposedly the same amount in all phases, one might expect that the volume trends would track the T^{2+} ionic sizes. For the most part this appears to be more or less true except for the iron phase whose unit cell volume is anomalously low. One possible explanation could be that a portion of the iron is present in the trivalent form.

Electrical Properties

The electrical resistivity of $La_5Mo_{3.3}Co_{0.7}O_{15.8}$ increases exponentially with decreasing temperature, which is indicative of semiconducting behavior, as shown in Fig. 9. The resistance of the sample below 110 K reaches 1.6×10^7 ohm, which is above the detection limit of our electronics used for the measurement. The room temperature resistivity of the Co-doped sample (1.4×10^4 ohm-cm) is, however, considerably higher than the corresponding value of $8.3. \times 10^{-1}$ ohm-cm observed for the undoped $La_5Mo_4O_{16}$ (2). Qualitative two-probe resistance measurements indicated

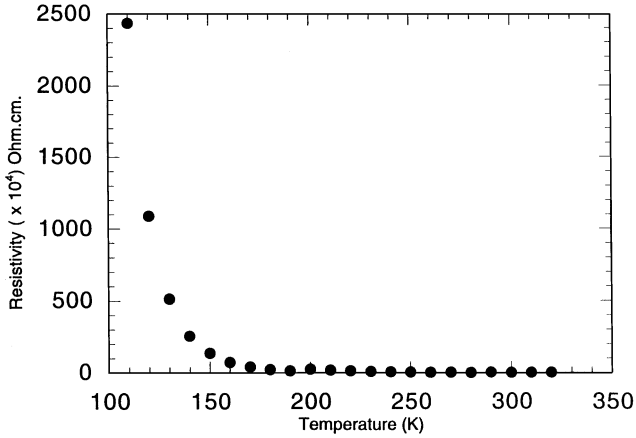

FIG. 9. Electrical resistivity vs temperature for $La_{5.00}Mo_{3.30}Co_{0.70}O_{15.8}$ crystals (current parallel to perovskite layers).

that all the substituted samples display similar resistance values at room temperature and hence no attempts were made to record their temperature dependence. The higher resistivity of the doped samples can be attributed to the disorder-induced localization of electrons due to the partial substitution of transition metals at the Mo(3) site.

Magnetic Properties

The magnetization data of randomly oriented single crystals of $La_5Mo_{3.3}Co_{0.7}O_{16}$ in the temperature range 2–400 K is shown in Fig. 10. As can be seen, the magnetization shows a sharp increase below 100 K and shows a maximum ~70 K. The observation of a maximum in the magnetization is also seen in the undoped $La_5Mo_4O_{16}$ crystals (see Fig. 4), however, at a somewhat higher temperature (~180 K). The AC and DC magnetic susceptibilities of

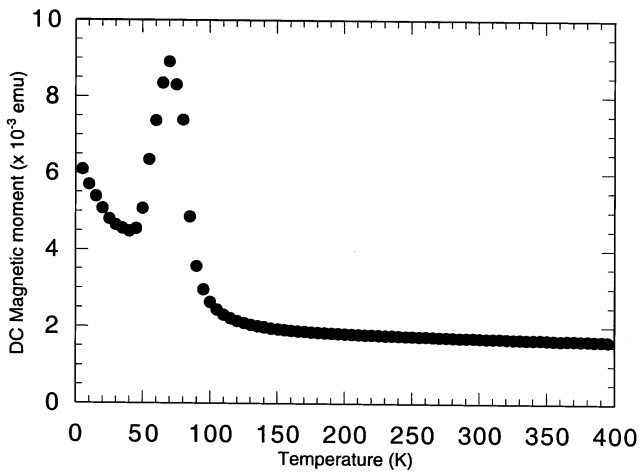

FIG. 10. Magnetization vs temperature of randomly oriented crystals of $La_5Mo_{3.31}Co_{0.69}O_{15.8}$.

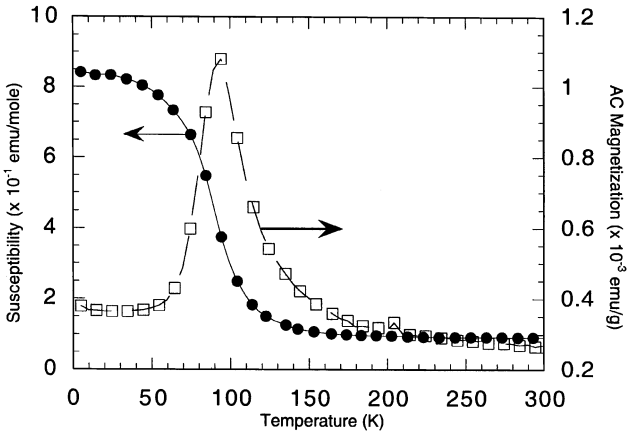

FIG. 11. AC and DC magnetic susceptibilities of $La_5Mo_{3.25}Co_{0.75}O_{15.25}$ powder as a function of temperature. Data were not corrected for the ferromagnetic Co particle impurities.

polycrystalline samples of Co-doped $La_5Mo_4O_{16}$ are shown in Fig. 11. The AC susceptibility shows a peak in the vicinity of ~100 K (suggestive of antiferromagnetic order) somewhat higher than that observed for the randomly oriented single crystals (Fig. 10), while the DC magnetization shows a sharp increase below 100 K followed by a saturation-like behavior at lower temperatures. It should, however, be remarked that the AC studies were carried out at much lower applied fields (10 G) compared to the DC measurement and hence the observed differences in their magnetization profiles may well point to metamagnetism. The nearly temperature-independent susceptibility in the range 100–200 K in AC and DC measurements of the sample may be explained in terms of the presence of a small amount of elemental Co particles which are ferromagnetic. In an effort to discern the true magnetic behavior of the samples, we have subtracted the contribution of Co metal particles by recording M–H loops at various temperatures. Assuming that the Co metal has a nearly constant ferromagnetic contribution in the temperature 2–400 K (T_c of Co is ~700°C, saturation moment is 7600 G), we have applied the correction to our DC susceptibility data and replotted it in Fig. 12. Following this correction, the data now appear to

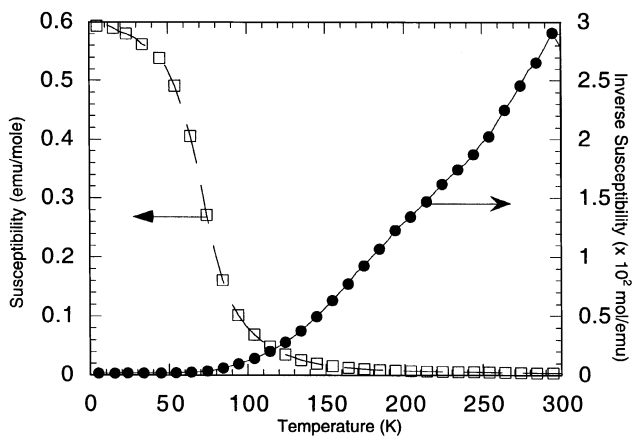

FIG. 12. Magnetic susceptibility and its inverse as a function of.temperature for $La_5Mo_{3.25}Co_{0.75}O_{15..25}$ powder, corrected for ferromagnetic impurity contribution.

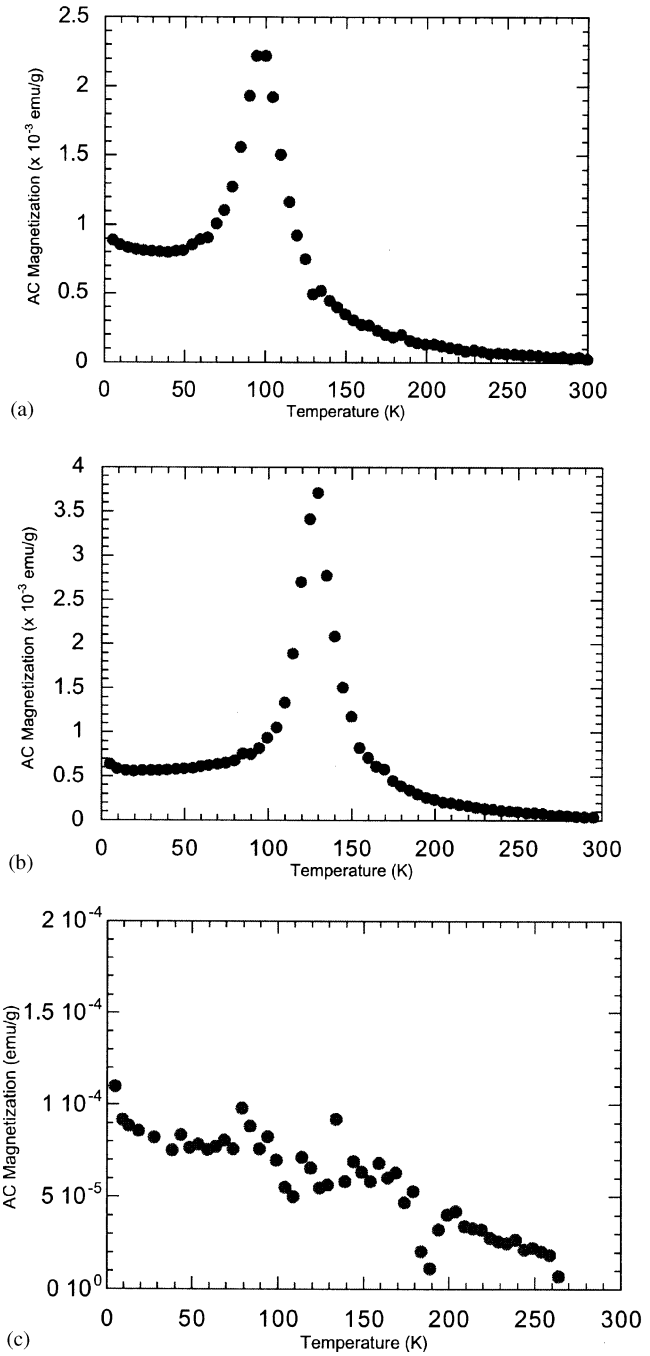

FIG. 13. AC magnetic susceptibility vs temperature for (a) $La_5Mo_{3.25}Mn_{0.75}O_{15.375}$, and (b) $La_5Mo_{3.25}Fe_{0.75}O_{15.375}$, and (c) $La_5Mo_{3.2}Mg_{0.8}O_{15}$. powders.

conform to Curie–Weiss behavior. However, a close inspection of the inverse susceptibility vs temperature plot reveals a small but noticeable deviation from ideal Curie–Weiss behavior at $\sim$200 K, which might arise from domains corresponding to the parent composition because of the incomplete substitution of Co at the Mo(3) site.

The AC and DC magnetic susceptibilities of doped $La_5Mo_4O_{16}$ samples with compositions $La_5Mo_{3.25}Mn_{0.75}O_{15.375}$, $La_5Mo_{3.25}Fe_{0.75}O_{15.375}$, and $La_5Mo_{3.3}Mg_{0.7}O_{15.8}$ are presented in Figs. 13a–13c. We also investigated the magnetic properties of $La_5Mo_{3.7}T_{0.3}O_{15.8}$ (T = Co, Mn, Fe, and Mg) phases and found no discernable changes in their magnetic ordering temperature. The Fe^{2+}- and Mn^{2+}-doped $La_5Mo_4O_{16}$ samples show features similar to those observed in the Co-doped composition; however, the maximum in the susceptibility varies with the dopant (for example, the Fe^{2+}-substituted samples display a maximum at $\sim$142 K, while the Mn^{2+} samples show a maximum at $\sim$110 K). As expected the Mg^{2+}-doped samples are weakly paramagnetic with no evidence of long-range magnetic order. A small kink in the magnetization data of Mg^{2+} samples at $\sim$180 K might be related to the presence of domains within the sample whose composition is similar to the pure $La_5Mo_4O_{16}$. This is to be expected because only 70% of the Mo(3) is replaced by Mg^{2+}.

Unlike the cobalt-substituted compounds, which are always contaminated with small amounts of ferromagnetic cobalt metal (both by solid-state and fused-salt electrolysis methods), samples containing Mn, Fe, and Mg did not show the presence of ferromagnetic impurities.

The field dependence of the magnetic anomaly observed in all the compositions studied here seems to indicate the presence of anisotropic metamagnetism wherein the in-plane (*ab*) correlations are ferromagnetic while the exchange correlations between the net moments of the successive *ab* planes are antiferromagnetic. In our earlier communication (2), we proposed a qualitative schematic of the 4*d* electronic density of states in Mo_2O_{10}, according to which the four electrons of Mo_2O_{10} unit are paired and stabilized in the bonding σ and π orbitals. Thus, the magnetic properties in this compound arise primarily from the in-plane Mo(2)–O–Mo(3) interactions which are predicted to be ferromagnetic. The observation of long-range magnetic order can be explained by invoking one of the two possibilities: (i) extended interactions between the moments of *ab* planes via the electrons of the Mo_2O_{10} bridge or (ii) exchange inversion taking place in the *ab* plane below T_N. Although the former is favored in the interpretation of the magnetic behavior of Mo_2O_{10}, it may not adequately account for the magnetization behavior of doped samples for two reasons: (i) Mo(2)–O–Mo(3) interactions are complicated by the presence of substitutional disorder at Mo(3) by the transition metal ions, (ii) partial oxidation of the Mo_2O_{10} unit results in a longer separation between Mo(1) atoms of the cluster. To address these issues further, we are currently examining the effect of compositional changes, in particular the T/Mo ratio and the oxygen nonstoichiometry on the overall magnetic properties of these phases. Nevertheless, detailed measurements of angle-dependent magnetization and neutron diffraction studies would be necessary to clarify the nature of interesting magnetic order observed in these systems.

ACKNOWLEDGMENTS

We acknowledge with pleasure the assistance of Project SEED scholars, Lyndon Stephenson, Jessica Ding, and Josephine Gerlaye, in some of the synthesis and analysis. K.V.R. acknowledges the support from Research Corporation (CC4366) and Rowan University through an award of a separately budgeted research grant. The work by W.H.M. and M.G. was supported by NSF Solid State Chemistry Grant DMR-99-07963.

REFERENCES

1. M. Ledesert, Ph. Labbe, W. H. McCarroll, H. Leligny, and B. Raveau, L., *J. Solid State Chem.* **105,** 143 (1993).
2. K. V. Ramanujachary, M. Greenblatt, W. H. McCarroll, and J. B. Goodenough, *Mater. Res. Bull.* **28,** 1256 (1993).
3. S. Lofland, K. V. Ramanujachary, and W. H. McCarroll, to be published.
4. C. R. Wiebe, A. Gourrier, T. Langet, J. F. Britten, and J. E. Greedan, *J. Solid State Chem.* **151,** 31 (2000).
5. W. H. McCarroll, C. Darling, and G. Jakubicki, *J. Solid State Chem.* **48,** 189 (1983).
6. A. Wold and D. Bellevance, *in* "Preparative Methods in Solid State Chemistry" (P. Hagenmuller, Ed.), pp. 297–308. Academic Press, New York, 1972.
7. CAD4Express Software, Enraf-Nonius, Delft, The Netherlands, 1994.
8. Sheldrick, G. M., SHELX76, Program for Crystal Structure Determination, Univ. of Cambridge, England, 1976.
9. Sheldrick, G. M., SHELXL97, Program for Crystal Structure Refinement, Univ. of Göttingen, Germany, 1997.
10. I. D. Brown and K. K. Wu, *Acta Crystallogr. Sect. B* **32,** 1957 (1976).
11. R. D. Shannon, *Acta Crystallogr. A* **32,** 751 (1976).